Clim. Past Discuss., 9, 1135–1164, 2013
www.clim-past-discuss.net/9/1135/2013/
doi:10.5194/cpd-9-1135-2013
© Author(s) 2013. CC Attribution 3.0 License.

Climate of the Past Discussions
Open Access

This discussion paper is/has been under review for the journal Climate of the Past (CP).
Please refer to the corresponding final paper in CP if available.

East Asian monsoon climate simulated in the PlioMIP

R. Zhang[1], Q. Yan[2], Z. S. Zhang[2,3], D. Jiang[1,2,4], B. L. Otto-Bliesner[5], A. M. Haywood[6], D. J. Hill[6,7], A. M. Dolan[6], C. Stepanek[8], G. Lohmann[8], C. Contoux[9,10], F. Bragg[11], W.-L. Chan[12], M. A. Chandler[13], A. Jost[10], Y. Kamae[14], A. Abe-Ouchi[12,15], G. Ramstein[9], N. A. Rosenbloom[5], L. Sohl[13], and H. Ueda[14]

[1]Climate Change Research Center, Chinese Academy of Sciences, Beijing 100029, China
[2]Nansen-Zhu International Research Centre, Institute of Atmospheric Physics, Chinese Academy of Sciences, Beijing 100029, China
[3]UniResearch, Bjerknes Centre for Climate Research, Bergen 5007, Norway
[4]Key Laboratory of Regional Climate-Environment Research for Temperate East Asia, Chinese Academy of Sciences, Beijing 100029, China
[5]National Center for Atmospheric Research, Boulder, Colorado, USA
[6]School of Earth and Environment, University of Leeds, Woodhouse Lane, Leeds, LS29JT, UK
[7]British Geological Survey, Keyworth, Nottingham, NG12 5GG, UK
[8]Alfred Wegener Institute, Helmholtz Centre for Polar and Marine Research, Bremerhaven, Germany
[9]LSCE/IPSL, CNRS-CEA-UVSQ, Saclay, France
[10]Sisyphe, CNRS/UPMC Univ Paris 06, Paris, France

[11]School of Geographical Sciences, University of Bristol, University Road, Bristol, BS8 1SS, UK
[12]Atmosphere and Ocean Research Institute, University of Tokyo, Kashiwa, Japan
[13]Columbia University – NASA/GISS, New York, NY, USA
[14]Graduate School of Life and Environmental Sciences, University of Tsukuba, Tsukuba, Japan
[15]Research Institute for Global Change, JAMSTEC, Yokohama, Japan

Received: 22 February 2013 – Accepted: 22 February 2013 – Published: 28 February 2013

Correspondence to: Z. S. Zhang (zhongshi.zhang@bjerknes.uib.no)

Published by Copernicus Publications on behalf of the European Geosciences Union.

CPD
9, 1135–1164, 2013

Abstract

Based on the simulations with fifteen climate models in the Pliocene Model Intercomparison Project (PlioMIP), the regional climate of East Asia (focusing on China) during the mid-Pliocene is investigated in this study. Compared to the pre-industrial, the multi-model ensemble mean (MMM) of all models shows the East Asian summer wind (EASW) largely strengthens in monsoon China, and the East Asian winter wind (EAWW) strengthens in south monsoon China but slightly weakens in north monsoon China in mid-Pliocene. The MMM of all models also illustrates a warmer and wetter mid-Pliocene climate in China. The simulated weakened mid-Pliocene EAWW in north monsoon China and intensified EASW in monsoon China agree well with geological reconstructions. However, the model-model discrepancy in simulating mid-Pliocene East Asian monsoon climate, in particular EAWW, should be further addressed in the future work of PlioMIP.

1 Introduction

The mid-Pliocene warm period (mPWP, 3.264 to 3.025 Ma), is the most recent time in Earth's history when global average temperature was warmer than modern but the paleogeography was similar to today (Dowsett et al., 2010). This warm period is thought to have many similarities to the projected warm climate of the late 21st century, as the global mean temperature is estimated to be 2–3 °C warmer than the pre-industrial (Haywood and Valdes, 2004). Thus, the study of this period is potentially important for understanding warm climate in the near future.

The mPWP has long been a focus for data syntheses (e.g., Dowsett et al., 1994, 1999, 2010; Salzmann et al., 2008) and climate modeling (e.g., Chandler et al., 1994; Jiang et al., 2005; Yan et al., 2011). The US geological survey's Pliocene Research Interpretation and Synoptic Mapping (PRISM) project (Dowsett et al., 1994, 1999, 2009, 2010) has studied this period for about 20 yr and the latest PRISM3 dataset has

CPD
9, 1135–1164, 2013

been released recently (Dowsett et al., 2010). Moreover, together with the progresses of mid-Pliocene reconstructions, the mid-Pliocene climate has been widely simulated with climate models (Chandler et al., 1994; Sloan et al., 1996; Haywood et al., 2000; Haywood and Valdes, 2004; Jiang et al., 2005; Lunt et al., 2010; Yan et al., 2011). Most of these simulations were carried out with atmospheric general circulation models (AGCMs) (Chandler et al., 1994; Sloan et al., 1996; Haywood et al., 2000; Jiang et al., 2005); only a few were carried out with coupled atmosphere–ocean general circulation models (AOGCMs) (Haywood and Valdes, 2004; Yan et al., 2011). In order to further understand the mPWP climate, the Pliocene Model Intercomparison Project (PlioMIP) was initiated and included in the Palaeoclimate Modeling Intercomparison Project (PMIP) phase III. In the PlioMIP, two types of experiments were designed (Haywood et al., 2010, 2011). One was performed with AGCMs and the other was performed with AOGCMs. Preliminary results from each model have been published in a special issue in Journal "Geoscientific Model Development" (see the references listed in Table 1).

Haywood et al. (2013) presented the first large-scale model-model intercomparison of PlioMIP simulations. They demonstrated that climate models differently interpreted the amount of forcing derived from Pliocene boundary conditions, and appeared able to reproduce many regional changes in temperature reconstructed from geological proxies (Haywood et al., 2013). This study focused on the model-model intercomparison on a global scale, but paid less attentions to regional climate, such as monsoon.

Monsoon is also an important topic included in the PlioMIP. Monsoon can be classified into two groups, tropical monsoon and subtropical monsoon. The tropical monsoon (e.g., Indian monsoon) is mainly driven by the seasonal movement of the intertropical convergence zone (Hoskins and Rodwell, 1995; Chao and Chen, 2001). The subtropical monsoon (e.g., East Asian monsoon) is further influenced by the land-sea thermal contrast (Ramage, 1971; Webster et al., 1998). Due to the different thermal capacity of the land and sea, the cold high-pressure system that occupies the inland Eurasian continent drives northwesterlies and northeasterlies in the East Asia during boreal winter

CPD
9, 1135–1164, 2013

(December, January and February, DJF), while the warm low-pressure system drives southwesterlies and southeasterlies and brings precipitation into East Asia during boreal summer (June, July and August, JJA).

In this study, we focus on the analyses of East Asian monsoon climate simulated in the PlioMIP. The investigation of tropical monsoon (e.g., Indian monsoon and African monsoon) will be presented in other studies. Moreover, since China is the largest country in East Asia, covering more than 80 % of the land area of East Asia, we focus on the monsoon climate over China here.

This paper is organized as follows: in Sect. 2, we present reconstructions of the mid-Pliocene climate in China. In Sect. 3, we briefly describe the models used in the PlioMIP and experimental design. Then we evaluate the simulations of pre-industrial climate with these models in China in Sect. 4. In Sect. 5, we analyze the mid-Pliocene climate changes including 850 hPa wind fields, surface air temperature (SAT) and precipitation, relative to the pre-industrial. Section 6 is discussion and summary.

2 Geological evidence for mid-Pliocene East Asian monsoon

In China, most mid-Pliocene geological evidences reveal changes in intensity of monsoon. Yan et al. (2012a) has summarized these mid-Pliocene proxy records that are well-dated by magnetostratigraphic and biostratigraphic chronology. The smaller mean/median grain size and proportion of coarse component (Xiong et al., 2001; Wan et al., 2007; Sun et al., 2008), the lower content of the 10–70 µm fraction (Jiang and Ding, 2010) in paleosol-loess sediments, together with the smaller abundance of *Neogloboquadrina dutertrei* in South China Sea ocean sediments (Jian et al., 2003; Li et al., 2004a) indicate East Asian winter winds (EAWW) were weaker during the mid-Pliocene, relative to the late Quaternary. Conversely, geochemical indices, including a larger ratio of free iron to total iron concentrations, larger proportion of finest end-member (fluvial mud) and smaller (illite + chlorite)/smectite ratio, indicated increased

CPD
9, 1135–1164, 2013

chemical weathering, thus suggesting intensified East Asian summer winds (EASW) (Ding et al., 2001; Wan et al., 2007).

Compared to these data of wind intensity, a few proxy data (Table 2) are found to be able to reconstruct temperature and humidity changes between mid-Pliocene and late Quaternary. These proxy data are classified into two groups according to the reliability in chronology and climate interpretation. In the first group, proxy data have good age control with a small age range between 3.0 and 3.3 Ma, and also a relatively reliable climate indication of temperature and/or humidity for the mid-Pliocene compared to the Late Quaternary (Ma et al., 2005; Wu et al., 2007; Jiang and Ding, 2008; Wu et al., 2011; Cai et al., 2012). In contrast, in the second group, the uncertainties in age control and/or climate interpretation are relatively large. The more reliable reconstructions in the first group indicate that it was warmer and wetter in China in the mid-Pliocene, relative to the Late Quaternary (Fig. S1).

In summary, these proxy data demonstrate that, during the warm mid-Pliocene period, the East Asian summer (winter) winds become stronger (weaker) than the Late Quaternary. These changes in winds are also supported by the records from the North Pacific ODP Site 885/886 (Rea et al., 1998), where received less aeolian sediments (low mass accumulation rate and smaller grain size) transported from inland Asia during the mid-Pliocene. On the other hand, it is highly likely that it was warmer and wetter in most of China during the mid-Pliocene relative to the Late Quaternary.

3 Models and experimental design

Nine climate modeling groups participated in the PlioMIP. Seven of them provide AGCMs simulations for PlioMIP Experiment 1 and eight groups provide AOGCMs simulations for PlioMIP Experiment 2 (Table 1). All simulations include a pre-industrial experiment and a mid-Pliocene experiment. Compared to the pre-industrial experiment, the changes of boundary conditions in the mid-Pliocene experiment include the modification in topography (Sohl et al., 2009), land cover (Salzmann et al., 2008) and

CPD
9, 1135–1164, 2013

the increase of atmospheric CO_2 concentration to 405 ppmv. AGCM simulations are forced with the fixed mid-Pliocene sea surface temperature (SST) (Dowsett et al., 2009; Robinson et al., 2011). Further details of boundary conditions and experimental design for the PlioMIP can be found in Haywood et al. (2010, 2011). Table 1 summarizes the implementation of the experimental set-up in each model.

4 Evaluation of the models

In order to know the model abilities in simulating East Asian monsoon climate, we evaluate the simulated winds, SAT and precipitation in pre-industrial experiment, with comparisons to the NCEP–DOE reanalysis data during the period 1979–2008 (Kanamitsu et al., 2002), the ERA40 monthly reanalysis data during the period 1972–2001 (Uppala et al., 2005) and the CMAP precipitation data during the period 1979–2008 (Xie and Arkin, 1996), respectively.

We regrid all model results and observations to the resolution of 2.5° × 2.5° (Fig. S2), and then calculate spatial correlation coefficient (SCC) and root-mean-square errors excluding systematic model error (RMSE). The SCC quantifies the similarity between simulated and observed spatial patterns. The larger SCC indicates the higher similarity. The RMSE assesses the internal model errors. The larger RMSE indicates the larger errors.

The SCC and RMSE of meridional wind at 850 hPa in the East Asian region of 20°–45° N and 105°–135°E show that the models used in the PlioMIP have a wide range of skills in simulating East Asian monsoon climate. As listed in Table S1, SCCs of EAWW are generally larger than SCCs of EASW, indicating that models have a better skill in simulating EAWW than EASW. For EASW, there are four models (CAM 3.1, MRI-CGCM2.3-AGCM, ECHAM5 and COSMOS) which show negative SCCs or in which confidence level of SCC is lower than 95 %.

The model ability in simulating East Asian monsoon climate shown above is also supported by the Taylor diagrams (Taylor, 2001) for meridional wind at 850 hPa (Fig. 1).

CPD
9, 1135–1164, 2013

The simulated EAWW points show less scatter around the point REF of observation than the simulated EASW points, indicating that the simulations of EAWW are better than those of EASW. For EASW (EAWW), the best model is ModelE2-R (HadAM3) with the highest SCC and smaller RMSE. The multi-model ensemble mean (MMM) point is close to the REF for both EASW and EAWW. So the MMM has a better skill than most individual models in simulating EASW and EAWW.

The models have different skills (Table S2) in simulating the pre-industrial annual and seasonal SAT over China. Compared to the observations, SCCs for annual and seasonal SAT in these pre-industrial simulations exceed 0.85, indicating these models can reasonably simulate SAT over China. The best model is HadAM3 with the highest SCC of approximately 0.99 and the smallest RMSE of 1.16 °C. In contrast, the range of the models' abilities is large in simulating the annual and seasonal precipitation over China. The best model is still HadAM3 with the highest SCC (0.91) and smaller RMSE (0.70 mm day^{-1}) for annual precipitation over China.

In the Taylor figures (Fig. 2), the simulated SAT points gather closely to the REF. In contrast, the precipitation points scatter and are far away from REF, indicating the larger discrepancies in simulating precipitation. Moreover, the MMM point is close to the REF, for both SAT and precipitation. Thus, the MMM is better than most individual simulations for SAT and precipitation over China. Two kinds of MMM are calculated, the unweighted and the weighted. The weighted MMM is based on weights taken from the SCC of each model. Regardless of whether the MMM is weighted or not, both have similar SCCs and similar RMSEs, indicating that the weights of these models are not important in calculating MMM of regional climate in China in the PlioMIP.

CPD
9, 1135–1164, 2013

5 Model-model intercomparison

5.1 Mid-Pliocene East Asian monsoon

Here, we use a classic indice, regionally averaged meridional wind speeds at 850 hPa (Wu and Ni, 1997; Wang et al., 2001) within the region of 20°–45° N and 105°–135° E to indicate the intensity of East Asian summer and winter winds. A positive (negative) indice represents southerly (northerly) wind anomalies, thus indicating intensified (weakened) EASW, or weakened (intensified) EAWW.

In the PlioMIP, the MMM indice of all models shows that the simulated mid-Pliocene EASW becomes stronger, and EAWW becomes slightly stronger, relative to the pre-industrial. In boreal summer, the mid-Pliocene MMM indice is 0.65 $m\,s^{-1}$ higher, and southwesterly anomalies (enhanced EASW) appears in monsoon China (Fig. 3a, Table 3). In boreal winter, the mid-Pliocene MMM indice is 0.06 $m\,s^{-1}$ lower than the pre-industrial. Northeasterly anomalies (enhanced EAWW) appear in south monsoon China, while weak southeasterly anomalies (weakened EAWW) occur in north monsoon China (Fig. 3b, Table 3).

Compared to the AOGCMs-MMM, the monsoon changes in AGCMs-MMM is in better agreement with those observed in the MMM of all models. The AOGCMs-MMM shows weaker intensification in the mid-Pliocene EASW (Fig. 3e vs. Fig. 3c), and further weakening (Fig. 3f vs. Fig. 3d) in the mid-Pliocene EAWW in north monsoon China, relative to the AGCMs-MMM.

For individual models, 14 simulations show increased indices in EASW, ranging from 0.12 $m\,s^{-1}$ (CCSM4) to 1.32 $m\,s^{-1}$ (HadAM3), while only COSMOS simulates a decreased indice of 0.30 $m\,s^{-1}$ (Table 3, Fig. S3). In contrast, the model-model discrepancies are much larger in simulating mid-Pliocene EAWW (Table 3, Fig. S4). The indice of EAWW decreases (indicating strengthened EAWW) in the simulations with CAM3.1, LMDZ5A, MRI-CGCM2.3-AGCM, ECHAM5, HadAM3, IPSLCM5A, MRI-CGCM2.3, COSMOS and CCSM4, but increases (indicating weakened EAWW) in

CPD
9, 1135–1164, 2013

the simulations with CAM4, MIROC4m-AGCM, NorESM-L, MIROC4m, HadCM3 and ModelE2-R.

As suggested by the reconstructions of the mid-Pliocene East Asian monsoon (see Sect. 2), if only the six models that simulate the weakened EAWW are considered, the obvious southeasterly anomalies occur in monsoon China in boreal winter (Fig. 3h). Moreover, the MMM of these six models also shows the mid-Pliocene EASW is further strengthened (Fig. 3g vs. Fig. 3a), when compared to the MMM of all models.

5.2 SAT

The MMM annual SAT averaged over China increases by 2.64 °C in the mid-Pliocene compared to the pre-industrial (Table 3). Stronger warming appears in western China. Regionally averaged SAT increases by 3.08 °C in western China and by 2.19 °C in monsoon China. In addition to the warming, small cooling areas appear in the Tarim basin and the south margin of Tibetan Plateau (Fig. 4a).

The changes in AGCMs-MMM or AOGCMs-MMM annual SAT are similar to the MMM of all models (Fig. 4c and e vs. Fig. 4a) over China, although the warming amplitude simulated with AOGCMs is slightly larger than AGCMs (Fig. 4e vs. Fig. 4c). The mid-Pliocene AOGCMs-MMM annual SAT regionally averaged over China is 3.05 °C higher than the pre-industrial. It is 0.88 °C greater than the SAT increase in the AGCMs-MMM.

For individual models, all models simulate warmer climates over China in the mid-Pliocene than the pre-industrial (Table 3, Fig. S5). The increases of annual SAT regionally averaged over China range from 1.46 °C (ModelE2-R) to 4.49 °C (HadCM3). Smaller scale changes in annual SAT in China are also captured by simulations, in particular the simulations with higher resolution AGCMs (Fig. S5).

The six models (CAM4, MIROC4m-AGCM, NorESM-L, MIROC4m, HadCM3 and ModelE2-R) that produce weakened EAWW generally simulate stronger mid-Pliocene warming over China than other models (Fig. 4g vs. Fig. 4a), particularly in boreal winter (Fig. 5c vs. Fig. 5a). As a result, further decreased land-sea thermal contrast in boreal

CPD
9, 1135–1164, 2013

winter, which causes the weakened EAWW, appears in the mid-Pliocene experiments simulated with these six models, when compared to other models (Fig. 6b).

5.3 Precipitation

The mid-Pliocene MMM annual precipitation averaged over China increases by 0.25 mm day^{-1}, relative to the pre-industrial. The annual MMM precipitation increases in most areas of China. However, decreased precipitation also can be observed in some small areas, for example in south monsoon China and the south margin of Tibetan Plateau (Fig. 4b).

The simulated changes in precipitation show similar patterns between AOGCMs-MMM and AGCMs-MMM over China (Fig. 4f vs. Fig. 4d). The increase in the mid-Pliocene MMM annual precipitation averaged over China is identical in the simulations with AGCMs (0.25 mm day^{-1}) and AOGCMs (0.25 mm day^{-1}).

For individual models, most models simulate an increased annual precipitation over China in the mid-Pliocene relative to the pre-industrial. The change in annual precipitation averaged over China ranges from −0.51 mm day^{-1} (COSMOS) to 0.75 mm day^{-1} (HadCM3), and only ECHAM5 and COSMOS simulate a decrease in annual precipitation. Although the changes in annual precipitation simulated with most models generally agree with the changes in MMM, these individual simulations still show considerable differences in spatial distribution (Fig. S7).

With the six models (CAM4, MIROC4m-AGCM, NorESM-L, MIROC4m, HadCM3 and ModelE2-R) that simulate the weakened EAWW, the precipitation increases in the mid-Pliocene MMM are larger than those in the MMM of all models (Fig. 4h vs. Fig. 4b). The more increases in precipitation are consistent with the further intensified EASW and weakened EAWW simulated with these six models (Fig. 6c and d).

CPD
9, 1135–1164, 2013

6 Discussion and summary

The above model-model intercomparisons show that the simulated mid-Pliocene EASW largely strengthens and the EAWW slightly enhances (Fig. 3a and b) in the MMM of all models, relative to the pre-industrial. When these models are classified into AGCMs and AOGCMs, the AOGCMs-MMM shows weaker intensified EASW, and further weakened EAWW in north monsoon China, relative to the AGCMs-MMM. Moreover, the MMM shows a warmer and wetter mid-Pliocene climate in most areas of China, which agrees with most reconstructed data (Fig. S1).

Although most models simulated intensified EASW, the model-model discrepancy in simulating mid-Pliocene EAWW can not be neglected. Nine models (CAM3.1, LMDZ5A, MRI-CGCM2.3-AGCM, ECHAM5, HadAM3, IPSLCM5A, MRI-CGCM2.3, COSMOS and CCSM4) reproduce intensified EAWW. On the contrary, six models (CAM4, MIROC4m-AGCM, NorESM-L, MIROC4m, HadCM3 and ModelE2-R) reproduce weakened EAWW. With these six models, when compared to other models, the further decreased land-sea thermal contrast caused the weakened EAWW in the mid-Pliocene experiments. Such change in the land-sea thermal contrast is controlled by the stronger mid-Pliocene warming in particular in boreal winter over China (Fig. 6b).

Compared to the mid-Pliocene monsoon reconstructions, the simulated weakened mid-Pliocene EAWW and intensified EASW agree better with geological evidence. The weakened EAWW reduces the dry airflow from inland Asia. Due to the weakened EAWW and wetter climate in the mid-Pliocene, the dust from arid inland Asia should have been reduced in the mid-Pliocene. As a result, dust accumulation rate was low on the Loess Plateau (Guo et al., 2002) and the mass accumulation rate and grain size in the ODP site 885/886 from North Pacific (Rea et al., 1998) was also low in the mid-Pliocene relative to the present.

It is interesting to notice that models in the PlioMIP have good skills in simulating EAWW in the pre-industrial control experiments, but show obvious discrepancies in simulating EAWW in the warm mid-Pliocene. In contrast, these models have relatively

CPD
9, 1135–1164, 2013

less skills in simulating EASW in the control experiments, but show almost consistent intensification in the mid-Pliocene EASW.

The reason behind this model behavior in simulating East Asian monsoon remains unclear. These models show different responses to the increased surface radiative forcing in the mid-Pliocene experiments. The different responses are likely related to independent physical processes and parameterizations in climate models. Moreover, according to the PlioMIP experimental design, the identical orbital parameters are used in the pre-industrial and the mid-Pliocene experiments. It is likely the heating over China during the mid-Pliocene is underestimated (in particular in boreal winter) in the simulations presented here. We also notice that the changes in topography boundary conditions are one possible reason for the discrepancy in simulating the mid-Pliocene EAWW, because the increase in mid-Pliocene topography boundary conditions (Fig. S8) weakens the warming magnitude simulated in China. The increased mid-Pliocene topography is not supported by geological evidence either, which demonstrates that there were uplifts on the margin of Tibetan Plateau since the mid-Pliocene (e.g., Li and Fang, 1999; Zheng et al., 2000; Fang et al., 2005). In addition, due to different model resolutions, smoothed or unsmoothed topography anomalies, which are used in creating mid-Pliocene topography conditions (Haywood et al., 2010, 2011, Fig. S8), may also bring some uncertainties in simulating East Asian monsoon climate. To better narrow the uncertainties, we suggest that more sensitivity experiments to the mid-Pliocene orbital parameters should be tested, and the modern topography (except for Greenland and Antarctic) can be potentially used, in the mid-Pliocene experiments of the PlioMIP phase II.

In summary, based on the PlioMIP multi-model intercomparison, the mid-Pliocene climate of East Asia (focusing on China) is investigated from simulations with the seven AGCMs (CAM3.1, HadAM3, LMDZ5A, MIROC4m-AGCM, MRI-CGCM2.3-AGCM, CAM4 and ECHAM5) and the eight AOGCMs (ModelE2-R, CCSM4, HadCM3, IPSLCM5A, MIROC4m, MRI-CGCM2.3, NorESM-L and COSMOS). The MMM of these models shows that EASW largely strengthens in monsoon China, and EAWW

CPD
9, 1135–1164, 2013

strengthens in south monsoon China, but slightly weakens in north monsoon China. The MMM of all these models also illustrates a warmer and wetter mid-Pliocene climate in China. The mid-Pliocene SAT averaged over China is 2.64 °C higher than the pre-industrial, with a range of levels from 1.46 °C to 4.49 °C among individual models. The mid-Pliocene precipitation averaged over China is 0.25 mm day^{-1} larger, with a range of levels from −0.51 mm day^{-1} to 0.75 mm day^{-1} among individual models. However, the model-model discrepancy in simulating mid-Pliocene East Asian climate, in particular the mid-Pliocene EAWW, can not be neglected. Six models simulated a weakened mid-Pliocene EAWW, whereas the other nine models did not. Although the simulation of weakened EAWW is supported by the mid-Pliocene geological evidence, the reason behind this discrepancy should be further addressed in the future work of PlioMIP.

Supplementary material related to this article is available online at: http://www.clim-past-discuss.net/9/1135/2013/cpd-9-1135-2013-supplement.pdf.

Acknowledgements. This study was jointly supported by the Strategic Priority Research Program of the Chinese Academy of Sciences (Grant No. XDB03020602), the Strategic and Special Frontier Project of Science and Technology of the Chinese Academy of Sciences (Grant No. XDA05080803) and the National 973 Program of China (Grant No. 2010CB950102). B. L. O. and N. A. R. acknowledge that the research and computing for this project were supported by the US National Science Foundation and Department of Energy. A. M. H. and A. M. D. acknowledge that the research leading to these results has received funding from the European Research Council under the European Union's Seventh Framework Programme (FP7/2007-2013)/ERC grant agreement no. 278636. A. M. D. acknowledges the UK Natural Environment Research Council (NERC) for the provision of a Doctoral Training Grant. D. J. H. acknowledges the Leverhulme Trust for the provision of an early career fellowship with financial contributions

CPD
9, 1135–1164, 2013

made by the National Centre for Atmospheric Science and the British Geological Survey. W.-L. C. and A. A.-O. acknowledge financial support from the Japan Society for the Promotion of Science and computing resources at the Earth Simulator Center, JAMSTEC. G. L. received funding through the Helmholtz research programme PACES and the Helmholtz Climate Initiative REKLIM. C. S. acknowledges financial support from the Helmholtz Graduate School for Polar and Marine Research and from REKLIM.

References

Bragg, F. J., Lunt, D. J., and Haywood, A. M.: Mid-Pliocene climate modelled using the UK Hadley Centre Model: PlioMIP Experiments 1 and 2, Geosci. Model Dev., 5, 1109–1125, doi:10.5194/gmd-5-1109-2012, 2012.

Cai, M. T., Fang, X. M., Wu, F. L., Miao, Y. F., and Appel, E.: Pliocene-Pleistocene stepwise drying of Central Asia: Evidence from paleomagnetism and sporopollen record of the deep borehole SG-3 in the western Qaidam Basin, NE Tibetan Plateau, Global Planet. Change, 94–95, 72–81, 2012.

Chan, W.-L., Abe-Ouchi, A., and Ohgaito, R.: Simulating the mid-Pliocene climate with the MIROC general circulation model: experimental design and initial results, Geosci. Model Dev., 4, 1035–1049, doi:10.5194/gmd-4-1035-2011, 2011.

Chandler, M., Rind, D., and Thompson, R.: Joint investigations of the middle Pliocene climate II: GISS GCM Northern Hemisphere results, Global Planet. Change, 9, 197–219, 1994.

Chandler, M. A., Sohl, L. E., Jonas, J. A., and Dowsett, H. J.: Simulations of the Mid-Pliocene Warm Period using the NASA/GISS ModelE2-R Earth System Model, Geosci. Model Dev. Discuss., 5, 2811–2842, doi:10.5194/gmdd-5-2811-2012, 2012.

Chao, W. C. and Chen, B.: The origin of monsoons, J. Atmos. Sci., 58, 3497–3507, 2001.

Contoux, C., Ramstein, G., and Jost, A.: Modelling the mid-Pliocene Warm Period climate with the IPSL coupled model and its atmospheric component LMDZ5A, Geosci. Model Dev., 5, 903–917, doi:10.5194/gmd-5-903-2012, 2012.

Ding, Z. L., Yang, S. L., Sun, J. M., and Liu, T. S.: Iron geochemistry of loess and red clay deposits in the Chinese Loess Plateau and implications for long-term Asian monsoon evolution in the last 7.0 Ma, Earth Planet. Sc. Lett., 185, 99–109, 2001.

CPD
9, 1135–1164, 2013

Dowsett, H. J., Thompson, R., Barron, J., Cronin, T., Fleming, F., Ishman, S., Poore, R., Willard, D., and Holtz, T.: Joint investigations of the middle Pliocene climate I: PRISM paleoenvironmental reconstructions, Global Planet. Change, 9, 169–195, 1994.

Dowsett, H. J., Barron, J. A., Poore, R. Z., Thompson, R. S., Cronin, T. M., Ishman, S. E., and Willard, D. A.: Middle Pliocene paleoenvironmental reconstruction: PRISM2, US Geol. Surv., Open File Rep., 99–535, 1999.

Dowsett, H. J., Robinson, M. M., and Foley, K. M.: Pliocene three-dimensional global ocean temperature reconstruction, Clim. Past, 5, 769–783, doi:10.5194/cp-5-769-2009, 2009.

Dowsett, H., Robinson, M., Haywood, A., Salzmann, U., Hill, D., Sohl, L., Chandler, M., Williams, M., Foley, K., and Stoll, D.: The PRISM3D paleoenvironmental reconstruction, Stratigraphy, 7, 123–139, 2010.

Eronen, J. T., Puolamaki, K., Liu, L., Lintulaakso, K., Damuth, J., Janis, C., and Fortelius, M.: Precipitation and large herbivorous mammals II: application to fossil data, Evol. Ecol. Res., 12, 235–248, 2010.

Fang, X. M., Zhao, Z. J., Li, J. J., Yan, M. D., Pan, B. T., Song, C. H., and Dai, S.: Magnetostratigraphy of the late Cenozoic Laojunmiao anticline in the northern Qilian Mountains and its implication for the northern Tibetan Plateau uplift, Sci. China Ser. D, 48, 1040–1051, 2005.

Guo, Z. T., Ruddiman, W. F., Hao, Q. Z., Wu, H. B., Qiao, Y. S., Zhu, R. X., Peng, S. Z., Wei, J. J., Yuan, B. Y., and Liu, T. S.: Onset of Asian desertifications by 22 Myr ago inferred from loess deposits in China, Nature, 416, 159–163, 2002.

Han, J., Fyfe, W. S., Longstaffe, F. J., Palmer, H. C., Yan, F. H., and Mai, X. S.: Pliocene-Pleistocene climatic change recorded in fluviolacustrine sediments in central China, Palaeogeogr. Palaeocl., 135, 27–39, 1997.

Hao, H., Ferguson, D. K., Chang, H., and Li, C. S.: Vegetation and climate of the Lop Nur area, China, during the past 7 million years, Climatic Change, 113, 323–338, 2012.

Haywood, A. M. and Valdes, P. J.: Modelling Pliocene warmth: contribution of atmosphere, oceans and cryosphere, Earth Planet. Sc. Lett., 218, 363–377, 2004.

Haywood, A. M., Sellwood, B. W., and Valdes, P. J.: Regional warming: Pliocene (3 Ma) paleoclimate of Europe and the Mediterranean, Geology, 28, 1063–1066, 2000.

Haywood, A. M., Dowsett, H. J., Otto-Bliesner, B., Chandler, M. A., Dolan, A. M., Hill, D. J., Lunt, D. J., Robinson, M. M., Rosenbloom, N., Salzmann, U., and Sohl, L. E.: Pliocene Model In-

CPD
9, 1135–1164, 2013

tercomparison Project (PlioMIP): experimental design and boundary conditions (Experiment 1), Geosci. Model Dev., 3, 227–242, doi:10.5194/gmd-3-227-2010, 2010.
Haywood, A. M., Dowsett, H. J., Robinson, M. M., Stoll, D. K., Dolan, A. M., Lunt, D. J., Otto-Bliesner, B., and Chandler, M. A.: Pliocene Model Intercomparison Project (PlioMIP): experimental design and boundary conditions (Experiment 2), Geosci. Model Dev., 4, 571–577, doi:10.5194/gmd-4-571-2011, 2011.
Haywood, A. M., Hill, D. J., Dolan, A. M., Otto-Bliesner, B. L., Bragg, F., Chan, W.-L., Chandler, M. A., Contoux, C., Dowsett, H. J., Jost, A., Kamae, Y., Lohmann, G., Lunt, D. J., Abe-Ouchi, A., Pickering, S. J., Ramstein, G., Rosenbloom, N. A., Salzmann, U., Sohl, L., Stepanek, C., Ueda, H., Yan, Q., and Zhang, Z.: Large-scale features of Pliocene climate: results from the Pliocene Model Intercomparison Project, Clim. Past, 9, 191–209, doi:10.5194/cp-9-191-2013, 2013.
Hoskins, B. J. and Rodwell, M. J.: A model of the Asian summer monsoon. Part I: The global scale, J. Atmos. Sci., 52, 1329–1340, 1995.
Jian, Z. M., Zhao, Q. H., Cheng, X. R., Wang, J. L., Wang, P. X., and Su, X.: Pliocene-Pleistocene stable isotope and paleoceanographic changes in the northern South China Sea, Palaeogeogr. Palaeocl., 193, 425–442, 2003.
Jiang, D., Wang, H. J., Ding, Z. L., Lang, X., and Drange, H.: Modeling the middle Pliocene climate with a global atmospheric general circulation model, J. Geophys. Res., 110, D14107, doi:14110.11029/12004JD005639, 2005.
Jiang, H. C. and Ding, Z. L.: A 20 Ma pollen record of East-Asian summer monsoon evolution from Guyuan, Ningxia, China, Palaeogeogr. Palaeocl., 265, 30–38, 2008.
Jiang, H. C. and Ding, Z. L.: Eolian grain-size signature of the Sikouzi lacustrine sediments (Chinese Loess Plateau): Implications for Neogene evolution of the East Asian winter monsoon, Geol. Soc. Am. Bull., 122, 843–854, 2010.
Kamae, Y. and Ueda, H.: Mid-Pliocene global climate simulation with MRI-CGCM2.3: set-up and initial results of PlioMIP Experiments 1 and 2, Geosci. Model Dev., 5, 793–808, doi:10.5194/gmd-5-793-2012, 2012.
Kanamitsu, M., Ebisuzaki, W., Woollen, J., Yang, S. K., Hnilo, J. J., Fiorino, M., and Potter, G. L.: NCEP-DOE AMIP-II reanalysis (R-2), B. Am. Meteorol. Soc., 83, 1631–1643, 2002.
Kou, X. Y., Ferguson, D. K., Xu, J. X., Wang, Y. F., and Li, C. S.: The reconstruction of paleovegetation and paleoclimate in the Late Pliocene of west Yunnan, China, Climatic Change, 77, 431–448, 2006.

CPD
9, 1135–1164, 2013

Li, B. H., Wang, J. L., Huang, B. Q., Li, Q. Y., Jian, Z. M., Zhao, Q. H., Su, X., and Wang, P. X.: South China Sea surface water evolution over the last 12 Myr: A south-north comparison from Ocean Drilling Program Sites 1143 and 1146, Paleoceanography, 19, PA1009, doi:1010.1029/2003PA000906, 2004a.
Li, J. J. and Fang, X. M.: Uplift of the Tibetan Plateau and environmental changes, Chinese Sci. Bull., 44, 2117–2124, 1999.
Li, X. Q., Li, C. S., Lu, H. Y., Dodson, J. R., and Wang, Y. F.: Paleovegetation and paleoclimate in middle-late Pliocene, Shanxi, central China, Palaeogeogr. Palaeocl., 210, 57–66, 2004b.
Liu, G. W., Leopold, E. B., Liu, Y., Wang, W. M., Yu, Z. Y., and Tong, G. B.: Palynological record of Pliocene climate events in North China, Rev. Palaeobot. Palyno., 119, 335–340, 2002.
Lunt, D. J., Haywood, A. M., Schmidt, G. A., Salzmann, U., Valdes, P. J., and Dowsett, H. J.: Earth system sensitivity inferred from Pliocene modelling and data, Nat. Geosci., 3, 60–64, 2010.
Ma, Y. Z., Wu, F. L., Fang, X. M., Li, J. J., An, Z. S., and Wang, W.: Pollen record from red clay sequence in the central Loess Plateau between 8.10 and 2.60 Ma, Chinese Sci. Bull., 50, 2234–2243, 2005.
Ramage, C. S.: Monsoon meteorology, Academic Press, New York, 1971.
Rea, D. K., Snoeckx, H., and Joseph, L. P.: Late Cenozoic eolian deposition in the north Pacific: Asian drying, Tibetan uplift, and cooling of the Northern Hemisphere, Paleoceanography, 15, 215–224, 1998.
Robinson, M. M., Valdes, P. J., Haywood, A. M., Dowsett, H. J., Hill, D. J., and Jones, S. M.: Bathymetric controls on Pliocene North Atlantic and Arctic sea surface temperature and deepwater production, Palaeogeogr. Palaeocl., 309, 92–97, 2011.
Rosenbloom, N. A., Otto-Bliesner, B. L., Brady, E. C., and Lawrence, P. J.: Simulating the mid-Pliocene Warm Period with the CCSM4 model, Geosci. Model Dev. Discuss., 5, 4269–4303, doi:10.5194/gmdd-5-4269-2012, 2012.
Salzmann, U., Haywood, A. M., Lunt, D. J., Valdes, P. J., and Hill, D. J.: A new global biome reconstruction and data-model comparison for the middle Pliocene, Global Ecol. Biogeogr., 17, 432–447, 2008.
Sloan, L. C., Crowley, T. J., and Pollard, D.: Modeling of middle Pliocene climate with the NCAR GENESIS general circulation model, Mar. Micropaleontol., 27, 51–61, 1996.

CPD
9, 1135–1164, 2013

Sohl, L. E., Chandler, M. A., Schmunk, R. B., Mankoff, K., Jonas, J. A., Foley, K. M., and Dowsett, H. J.: PRISM3/GISS topographic reconstruction, US Geol. Surv. Data Serie 419, 2009.

Stepanek, C. and Lohmann, G.: Modelling mid-Pliocene climate with COSMOS, Geosci. Model Dev., 5, 1221–1243, doi:10.5194/gmd-5-1221-2012, 2012.

Sun, B. N., Wu, J. Y., Liu, Y. S., Ding, S. T., Li, X. C., Xie, S. P., Yan, D. F., and Lin, Z. C.: Reconstructing Neogene vegetation and climates to infer tectonic uplift in western Yunnan, China, Palaeogeogr. Palaeocl., 304, 328–336, 2011.

Sun, D. H., Su, R. X., Bloemendal, J., and Lu, H. Y.: Grain-size and accumulation rate records from Late Cenozoic aeolian sequences in northern China: Implications for variations in the East Asian winter monsoon and westerly atmospheric circulation, Palaeogeogr. Palaeocl., 264, 39–53, 2008.

Taylor, K. E.: Summarizing multiple aspects of model performance in a single diagram, J. Geophys. Res., 106, 7183–7192, 2001.

Uppala, S. M., Kallberg, P. W., Simmons, A. J., Andrae, U., Bechtold, V. D., Fiorino, M., Gibson, J. K., Haseler, J., Hernandez, A., Kelly, G. A., Li, X., Onogi, K., Saarinen, S., Sokka, N., Allan, R. P., Andersson, E., Arpe, K., Balmaseda, M. A., Beljaars, A. C. M., Van De Berg, L., Bidlot, J., Bormann, N., Caires, S., Chevallier, F., Dethof, A., Dragosavac, M., Fisher, M., Fuentes, M., Hagemann, S., Holm, E., Hoskins, B. J., Isaksen, L., Janssen, P. A. E. M., Jenne, R., McNally, A. P., Mahfouf, J. F., Morcrette, J. J., Rayner, N. A., Saunders, R. W., Simon, P., Sterl, A., Trenberth, K. E., Untch, A., Vasiljevic, D., Viterbo, P., and Woollen, J.: The ERA-40 re-analysis, Q. J. Roy. Meteorol. Soc., 131, 2961–3012, 2005.

Wan, S. M., Li, A. C., Clift, P. D., and Stuut, J. B. W.: Development of the East Asian monsoon: Mineralogical and sedimentologic records in the northern South China Sea since 20 Ma, Palaeogeogr. Palaeocl., 254, 561–582, 2007.

Wang, W. M., Li, J. R., Wang, J. D., and He, Z. J.: Palynofloras from Pliocene balouhe formation and Pleistocene in Zhangqiu County, Shandong Province, Acta Palaeonotol. Sin., 41, 72–76, 2002 (in Chinese with English abstract).

Wang, Y. F., Wang, B., and Oh, J.-H.: Impacts of the preceding El Niño on the East Asian summer atmospheric circulation, J. Meteor. Soc. Jpn., 79, 575–588, 2001.

Webster, P. J., Magaña, V. O., Palmer, T. N., Shukla, J., Tomas, R. A., Yanai, M., and Yasunari, T.: Monsoons: Processes, predictability, and the prospects for prediction, J. Geophys. Res., 103, 14451–14510, 1998.

CPD
9, 1135–1164, 2013

Wu, A. and Ni, Y.: The influence of Tibetan Plateau on the interannual variability of Asian monsoon, Adv. Atmos. Sci., 14, 491–504, 1997.
Wu, F. L., Fang, X., Ma, Y., Herrmann, M., Mosbrugger, V., An, Z., and Miao, Y.: Plio-Quaternary stepwise drying of Asia: Evidence from a 3-Ma pollen record from the Chinese Loess Plateau, Earth Planet. Sc. Lett., 257, 160–169, 2007.
Wu, F. L., Fang, X. M., Herrmann, M., Mosbrugger, V., and Miao, Y. F.: Extended drought in the interior of Central Asia since the Pliocene reconstructed from sporopollen records, Global Planet. Change, 76, 16–21, 2011.
Wu, N. Q., Pei, Y. P., Lu, H. Y., Guo, Z. T., Li, F. J., and Liu, T. S.: Marked ecological shifts during 6.2–2.4 Ma revealed by a terrestrial molluscan record from the Chinese Red Clay Formation and implication for palaeoclimatic evolution, Palaeogeogr. Palaeocl., 233, 287–299, 2006.
Wu, Y. S.: Palynoflora at late Miocene-early Pliocene from leijiahe of lingtai, Gansu Province, China, Acta Bot. Sin., 43, 750–756, 2001 (in Chinese with English abstract).
Xie, P. P. and Arkin, P. A.: Analyses of global monthly precipitation using gauge observations, satellite estimates, and numerical model predictions, J. Climate, 9, 840–858, 1996.
Xie, S., Sun, B., Wu, J., Lin, Z., Yan, D., and Xiao, L.: Palaeoclimatic estimates for the Late Pliocene based on leaf physiognomy from western Yunnan, China, Turk. J. Earth Sci., 21, 251–261, 2012.
Xiong, S. F., Ding, Z. L., and Yang, S. L.: Abrupt shifts in the late Cenozoic environment of north-western China recorded in loess-palaeosol-red clay sequences, Terra Nova, 13, 376–381, 2001.
Yan, Q., Zhang, Z. S., Wang, H. J., Jiang, D., and Zheng, W. P.: Simulation of sea surface temperature changes in the middle Pliocene warm period and comparison with reconstructions, Chinese Sci. Bull., 56, 890–899, 2011.
Yan, Q., Zhang, Z. S., and Gao, Y. Q.: An East Asian monsoon in the mid-Pliocene, Atmos. Ocean. Sc. Lett., 5, 449–454, 2012a.
Yan, Q., Zhang, Z. S., Wang, H. J., Gao, Y. Q., and Zheng, W. P.: Set-up and preliminary results of mid-Pliocene climate simulations with CAM3.1, Geosci. Model Dev., 5, 289–297, doi:10.5194/gmd-5-289-2012, 2012b.
Yao, Y. F., Bruch, A. A., Cheng, Y. M., Mosbrugger, V., Wang, Y. F., and Li, C. S.: Monsoon versus uplift in southwestern China – Late Pliocene climate in Yuanmou Basin, Yunnan, PLoS ONE, 7, e37760, doi:37710.31371/journal.pone.0037760, 2012.

CPD
9, 1135–1164, 2013

Zhang, Z. and Yan, Q.: Pre-industrial and mid-Pliocene simulations with NorESM-L: AGCM simulations, Geosci. Model Dev., 5, 1033–1043, doi:10.5194/gmd-5-1033-2012, 2012.

Zhang, Z. S., Nisancioglu, K., Bentsen, M., Tjiputra, J., Bethke, I., Yan, Q., Risebrobakken, B., Andersson, C., and Jansen, E.: Pre-industrial and mid-Pliocene simulations with NorESM-L, Geosci. Model Dev., 5, 523-533, doi:10.5194/gmd-5-523-2012, 2012.

Zhang, Z. S., Nisancioglu, K. H., and Ninnemann, U. S.: Increased ventilation of Antarctic deep water during the warm mid-Pliocene, Nat. Commun., 4, 1499, doi:10.1038/ncomms2521, 2013.

Zhao, L. C., Collinson, M. E., and Li, C. S.: Fruits and seeds of *Ruppia* (Potamogetonaceae) from the Pliocene of Yushe Basin, Shanxi, northern China and their ecological implications, Bot. J. Linn. Soc., 145, 317–329, 2004.

Zheng, H. B., Powell, C. M., and An, Z. S.: Pliocene uplift of the northern Tibetan Plateau, Geology, 28, 715–718, 2000.

CPD
9, 1135–1164, 2013

Table 1. Basic information of GCMs used in this paper.

Model	Type	Boundary condition	Atmosphere resolution	Years for analyzing	References
CAM3.1	AGCM	alternate	T42, L26	30	Yan et al. (2012b)
HadAM3	AGCM	preferred	2.5° × 3.75°, L19	30	Bragg et al. (2012)
LMDZ5A	AGCM	alternate	1.9° × 3.75°, L39	30	Contoux et al. (2012)
MIROC4m-AGCM	AGCM	preferred	T42, L20	30	Chan et al. (2011)
MRI-CGCM2.3-AGCM	AGCM	alternate	T42, L30	50	Kamae and Ueda (2012)
CAM4	AGCM	alternate	T31, L26	20	Zhang and Yan (2012)
ECHAM5	AGCM	preferred	T31, L19	30	Stepanek and Lohmann (2012)
ModelE2-R	AOGCM	preferred	2° × 2.5°, L40	30	Chandler et al. (2012)
CCSM4	AOGCM	alternate	0.9° × 1.25°, L26	30	Rosenbloom et al. (2012)
HadCM3	AOGCM	alternate	2.5° × 3.75°, L19	50	Bragg et al. (2012)
IPSLCM5A	AOGCM	alternate	1.9° × 3.75°, L39	30	Contoux et al. (2012)
MIROC4m	AOGCM	preferred	T42, L20	30	Chan et al. (2011)
MRI-CGCM2.3	AOGCM	alternate	T42, L30	50	Kamae and Ueda (2012)
NorESM-L	AOGCM	alternate	T31, L26	100	Zhang et al. (2012, 2013)
COSMOS	AOGCM	preferred	T31, L19	30	Stepanek and Lohmann (2012)

CPD
9, 1135–1164, 2013

Table 2. Data used to reconstruct the mid-Pliocene climate in China.

No	Site	Proxy data	Dating	Location	Age (Ma)	Geological records (Compared to the Late Quaternary)	Reconstructed climate	References
First group								
1	Sikouzi, Gansu	Pollen	Paleomagnetism, biostratigraphy	36°16′ N, 105°59′ E	3.3–3.0	More tree and shrubs, less herbs	Wetter	Jiang and Ding (2008)
2	Chaona, Gansu	Pollen	Paleomagnetism	35°7′ N, 107°12′ E	3.0–2.6	A domination of typical Cupressaceae forest vegetation	Warmer and wetter	Wu et al. (2007)
	Chaona, Gansu	Pollen	Paleomagnetism	35°7′ N, 107°21′ E	3.3–3.0	The predominance of Cupressaceae and *Juniperus* with lower *Ulmus*	Warmer and wetter	Ma et al. (2005)
3	Qaidam Basin	Sporopollen	Paleomagnetism	38°22′ N, 91°44′ E	3.1–3.0	Higher abundance of broadleaved trees and lower abundance of Xerophytic taxa	Warmer and wetter	Cai et al. (2012)
4	Qaidam Basin	Sporopollen	Paleomagnetism, biostratigraphy	~37.8° N, ~94.8° E	3.3–3.0	Low fraction of Xerophytic plants and the existence of thermophilous subtropical trees	Warmer and wetter	Wu et al. (2011)
Second group								
5	Yushe, Shanxi	Pollen	Paleomagnetism	~37° N, ~113° E	3.2–3.0	Contains various thermophiles, e.g. *Carya*, *Juglans*, etc. These thermophilic taxa are now present about 1 or 2 latitude degrees south of the Yushe Basin	Warmer	Liu et al. (2002)
6	Yushe, Shanxi	Fruits, seeds	Paleomagnetism	36°58′ N, 112°50′ E	3.5–2.3	The existence of lake and *Ruppia*	Wetter	Zhao et al. (2004)
7	Taigu and Yushe, Shanxi	Pollen	Paleomagnetism	~37.5° N, ~114° E	3.6–2.5	The high percentages of *Picea* and *Abies*, and the absence of thermophiles in pollen assemblages	Colder and wetter	Li et al. (2004b)
8	Shijiawan, Shaanxi	Pollen	Paleomagnetism	~34.4° N, ~109.7° E	3.0–2.7	Typical steppe type; with elephant fossil fauna	Warmer and drier	Han et al. (1997)
9	Xifeng, Gansu	Molluscan	Paleomagnetism	35°53′ N, 107°58′ E	3.4–2.4	Increase of coldaridiphilous taxa, decrease of meso-xerophilous and the rare occurrence of thermo-humidiphilous mollusks	Colder and drier	Wu et al. (2006)
10	Lingtai, Gansu	Sporopollen	Paleomagnetism, biostratigraphy	35°04′ N, 107°43′ E	5.8–3.4	The existence of some subtropical trees	Warmer and wetter	Wu (2001)
11	Eastern China	Fossil mammals	Stratigraphy	32° N, 105° E*	3.4–2.0	High hypsodonty	Drier	Eronen et al. (2010)
12	Yuanmou, Yunan			~25.7° N, ~101.9° E	3.4–2.5	Based on coexistence approach	Colder and wetter	Yao et al. (2012)
13	Tuantian, Yunan			24°41′ N, 98°37′ E	3.3–2.3	Based on Leaf Margin Analysis and the Climate-Leaf Analysis Multivariate Program	Warmer and drier	Xie et al. (2012)
14	Tengchong, Yunnan	Fossil woods, leaves, pollen	Paleomagnetism, K-Ar and Rb-Sr biostratigraphy,	~24.7° N, ~98.4° E			Warmer	
15	Eryuan, Yunnan		lithostratigraphy, isotopic dating	26°00′ N, 99°49′ E	Late Pliocene	Based on coexistence approach	Warmer	Kou et al. (2006); Sun et al. (2011)
16	Yangyi, Yunnan			24°57′ N, 99°15′ E			Warmer and wetter	
17	Longling, Yunnan			24°41′ N, 98°50′ E			Warmer and drier	
18	Zhangqiu, Shandong	Pollen	Biostratigraphy	36°43′ N, 117°27′ E	Pliocene	The distribution of a few subtropical and warm temperate broadleaf trees	Warmer and wetter	Wang et al. (2002)
19	Lop Nur, Xinjiang	Sporopollen	Paleomagnetism	39°47′ N, 88°23′ E	Pliocene	Based on coexistence approach	Warmer and wetter	Hao et al. (2012)

* Only take one point (32° N, 105° E).

CPD
9, 1135–1164, 2013

Table 3. The regionally averaged changes of EAWW, EASW, SAT and precipitation between mid-Pliocene and pre-industrial experiments. The EAWW and EASW changes (units: $m\,s^{-1}$) are calculated by regionally averaged meridional wind speed at 850 hPa within the region of 20°–45° N and 105°–135° E. The SAT (units: °C) and precipitation (units: $mm\,day^{-1}$) changes are calculated by regionally averaged values within China.

			SAT			Precipitation		
Model	EASW	EAWW	ANN	JJA	DJF	ANN	JJA	DJF
CAM3.1	0.58	−0.20	1.50	1.48	1.54	0.17	−0.09	0.02
HadAM3	1.32	−0.30	1.84	1.35	2.16	0.45	0.50	0.12
LMDZ5A	0.82	−0.37	2.05	2.12	1.79	0.18	0.37	−0.01
MIROC4m-AGCM	0.99	0.02	2.97	1.57	4.10	0.52	0.42	0.13
MRI-CGCM2.3-AGCM	1.27	−0.22	2.04	0.91	3.33	0.27	0.36	−0.12
CAM4	0.77	0.67	2.70	1.68	3.66	0.27	0.07	0.04
ECHAM5	0.56	−0.45	2.05	1.41	3.11	−0.10	−0.73	−0.08
ModelE2-R	0.43	0.28	1.46	2.86	0.37	0.17	0.71	−0.15
CCSM4	0.12	−0.09	2.24	1.92	2.60	0.20	0.05	0.25
HadCM3	1.20	0.84	4.49	4.17	5.45	0.75	0.83	0.37
IPSLCM5A	0.22	−0.36	2.28	2.22	2.18	0.24	0.47	0.07
MIROC4m	1.07	0.94	4.08	3.37	4.66	0.63	0.47	0.31
MRI-CGCM2.3	0.36	−0.33	2.06	1.33	2.99	0.20	0.24	−0.02
NorESM-L	0.31	0.17	3.43	2.32	4.50	0.33	0.24	0.12
COSMOS	−0.30	−1.53	4.34	4.08	4.91	−0.51	−0.77	−0.33
MMM	0.65	−0.06	2.64	2.18	3.16	0.25	0.21	0.05
AGCMs-MMM	0.90	−0.12	2.17	1.50	2.81	0.25	0.13	0.01
AOGCMs-MMM	0.43	0.00	3.05	2.78	3.46	0.25	0.28	0.08

CPD
9, 1135–1164, 2013

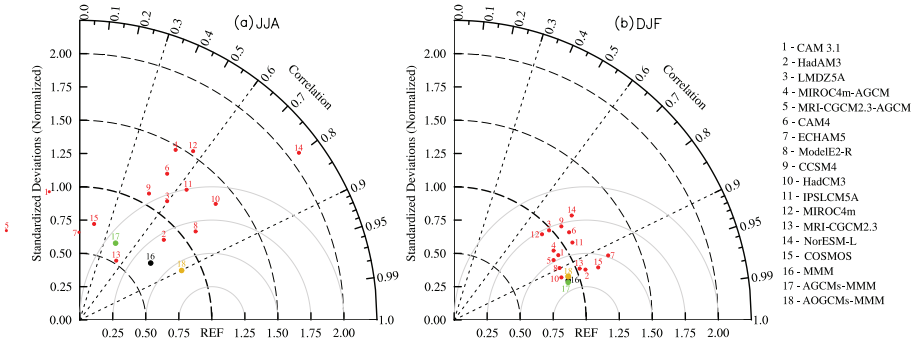

Fig. 1. Taylor diagrams of **(a)** summer and **(b)** winter meridional wind at 850 hPa in the East Asian regions of 20°–45° N and 105°–135° E for different models. The point of REF indicates the NCEP–DOE reanalysis data averaged within 1979–2008 (Kanamitsu et al., 2002). In the Taylor diagram, the standard deviation of the modelled field is the radial distance from the origin. The RMSE is the distance to the REF point. The azimuthal position gives the SCC. The RMSE and the modelled standard deviation are normalized by the observed standard deviation.

CPD
9, 1135–1164, 2013

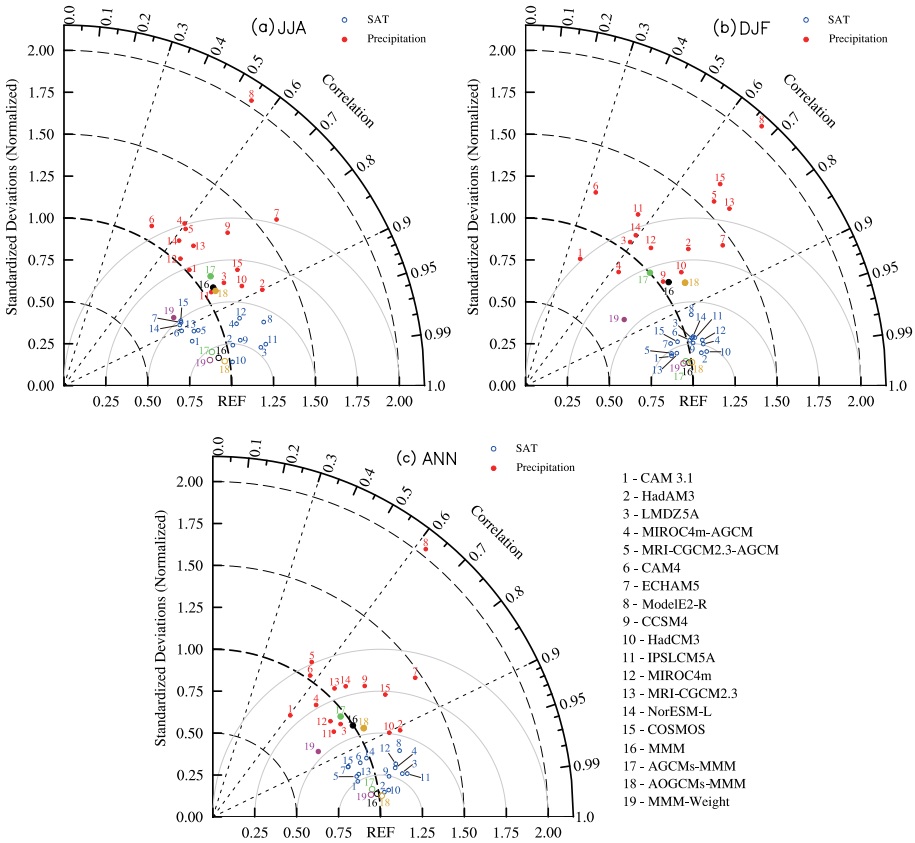

Fig. 2. Taylor diagrams of **(a)** summer, **(b)** winter and **(c)** annual mean SAT and precipitation in China for different models. The point of "REF" indicates the ERA40 reanalysis data averaged within 1972–2001 (Uppala et al., 2005) for SAT or the CMAP data averaged within 1979–2008 (Xie and Arkin, 1996) for precipitation.

CPD
9, 1135–1164, 2013

East Asian monsoon climate simulated in the PlioMIP

R. Zhang et al.

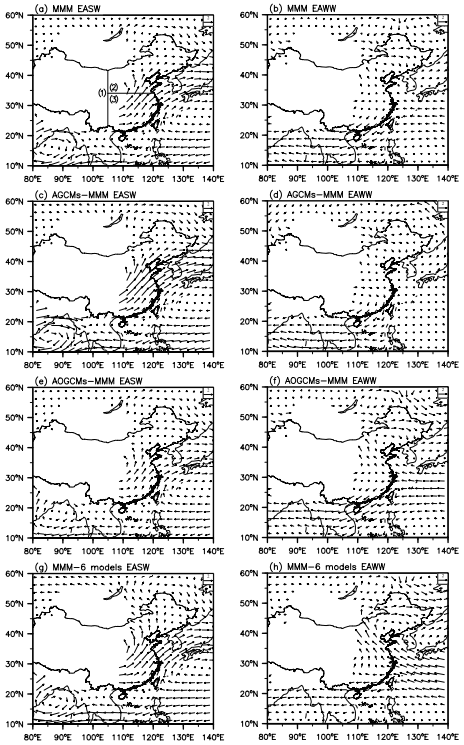

Fig. 3. The MMM for EASW (left column, units: $m\,s^{-1}$) and EAWW differences (right column, units: $m\,s^{-1}$) between mid-Pliocene and pre-industrial experiments. **(a)** and **(b)** are the MMM of all models, **(c)** and **(d)** are the AGCMs-MMM, **(e)** and **(f)** are the AOGCMs-MMM, **(g)** and **(h)** are the MMM of the six models that simulate the weakened EAWW listed in Table 3. In **(a)**, region (1), (2) and (3) represent the western China, the north monsoon China and the south monsoon China, respectively. Region (2) and (3) together represent monsoon China. Regions with an elevation above 1500 m are left blank.

CPD
9, 1135–1164, 2013

East Asian monsoon climate simulated in the PlioMIP

R. Zhang et al.

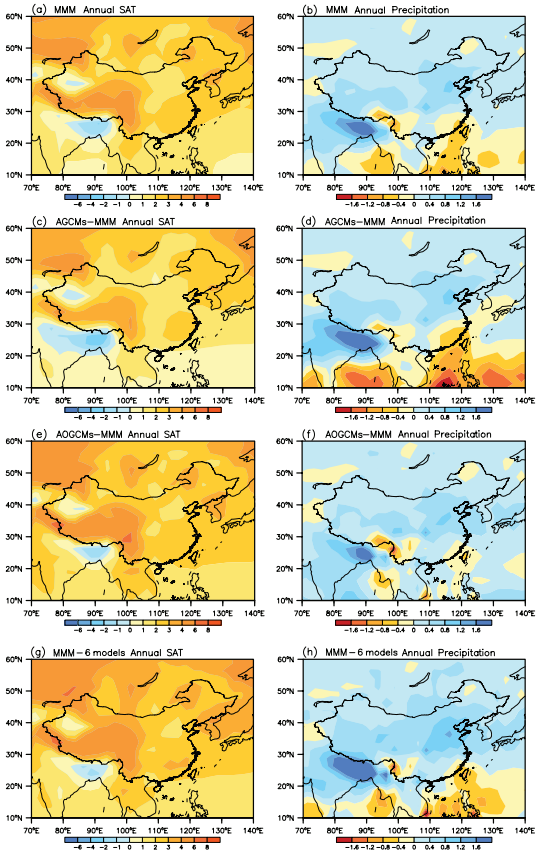

Fig. 4. Same as Fig. 3, but for annual mean SAT (left column, units: ˚C) and precipitation differences (right column, units: mm day^{-1}). The standard deviation of the simulated annual SAT and precipitation changes can be seen in Fig. S6.

CPD
9, 1135–1164, 2013

East Asian monsoon climate simulated in the PlioMIP

R. Zhang et al.

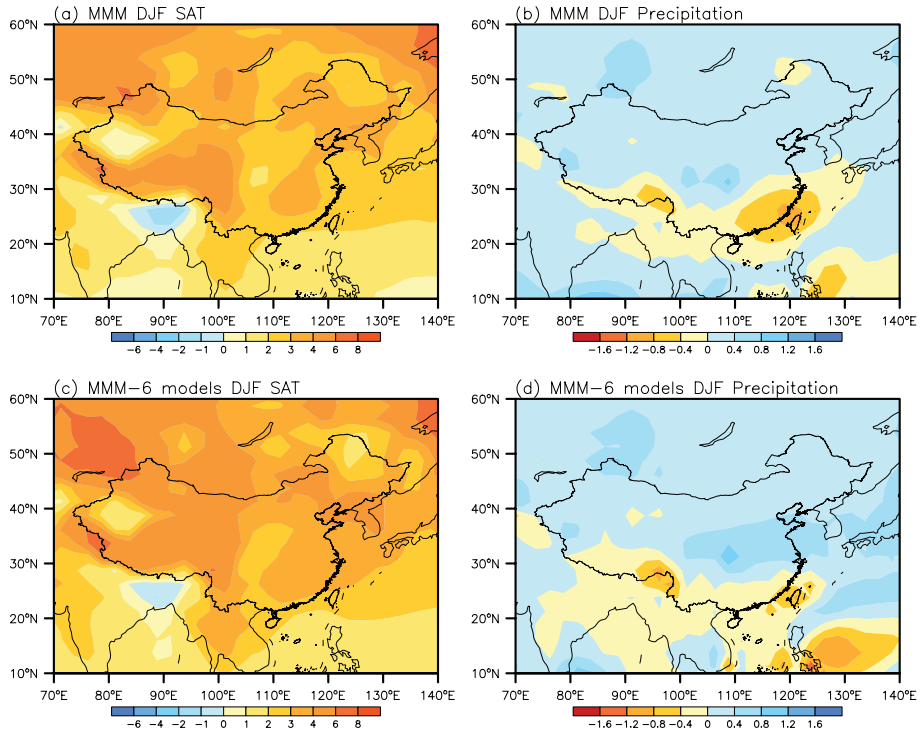

Fig. 5. The MMM for winter SAT (left column, units: °C) and precipitation differences (right column, units: mm day^{-1}) between mid-Pliocene and pre-industrial experiments. **(a)** and **(b)** are the MMM of all models, **(c)** and **(d)** are the MMM of the six models that simulate the weakened EAWW listed in Table 3.

CPD
9, 1135–1164, 2013

East Asian monsoon climate simulated in the PlioMIP

R. Zhang et al.

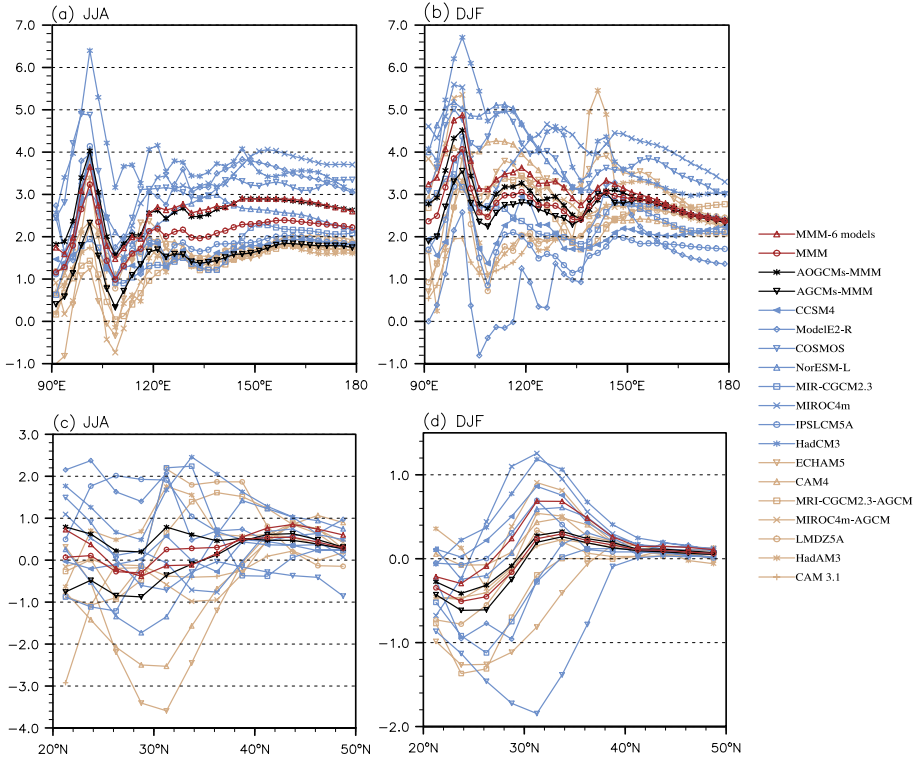

Fig. 6. The seasonal SAT (top, units: ˚C) and precipitation differences (bottom, units: mm day^{-1}) between mid-Pliocene and pre-industrial experiments. The SAT changes are longitudinally averaged within 20˚–50˚ N. The precipitation changes are zonally averaged within 105˚–120˚ E.

CPD
9, 1135–1164, 2013

East Asian monsoon climate simulated in the PlioMIP

R. Zhang et al.